# Rotational bands near the $Z$=50 closed shell: $^{111}_{51}$Sb

D.R. LaFosse, D.B. Fossan, J.R. Hughes,* Y. Liang,† H. Schnare, P. Vaska, M.P. Waring, and J.-y. Zhang‡
*Department of Physics, State University of New York at Stony Brook, Stony Brook, New York 11794*

R.M. Clark§ and R. Wadsworth
*Department of Physics, University of York, Heslington, York YO1 5DD, United Kingdom*

S.A. Forbes and E.S. Paul
*Oliver Lodge Laboratory, University of Liverpool, P.O. Box 147, Liverpool L69 3BX, United Kingdom*

V.P. Janzen, A. Galindo-Uribarri, D.C. Radford, and D. Ward
*AECL Research, Chalk River Laboratories, Chalk River, Ontario, Canada K0J 1J0*

S.M. Mullins and D. Prévost‖
*Department of Physics and Astronomy, McMaster University, Hamilton, Ontario, Canada L8S 4M1*

G. Zwartz
*Department of Physics, University of Toronto, Ontario, Canada M5S 1A7*
(Received 4 April 1994)

Rotational states have been identified in $^{111}_{51}$Sb for the first time. Three decoupled ($\Delta I$=2) bands extending to over 1 MeV in rotational frequency have been observed. At the highest frequencies, the $\mathcal{J}^{(2)}$ moments of inertia for these three bands are seen to decrease steadily to unexpectedly low values; this is interpreted as evidence for a novel form of band termination. One of these bands is interpreted as being based on the $\pi h_{11/2}$ orbital coupled to a deformed $[(\pi g_{9/2})^{-2}\otimes(\pi g_{7/2})^2]_{0^+}$ state of the $^{110}_{50}$Sn core. The interaction strength for the alignment of a pair of $h_{11/2}$ neutrons has been extracted and compared with calculations. Two possible quasiparticle configurations are discussed for the other decoupled bands. Two strongly coupled ($\Delta I$=1) bands have been identified and both shown to involve the $[(\pi g_{9/2})^{-1}\otimes(\pi g_{7/2})^2]$ configuration. A large number of spherical states have also been observed, which can be explained on the basis of valence protons coupled to spherical states in the $^{110}$Sn core.

PACS number(s): 21.10.Re, 27.60.+j, 23.20.Lv

## I. INTRODUCTION

The study of collective structures in nuclei near the $Z$=50 closed shell has recently enjoyed an upsurge in activity. Because of the influence of the large proton shell gap, $_{50}$Sn and $_{51}$Sb nuclei are expected to show predominantly spherical excitations at low excitation energies. Indeed, the level schemes of odd Sb nuclei show a large number of states which consist simply of a single proton orbital coupled to spherical states of the neighboring even Sn core. The even Sn nuclei have rigid spherical ground states with the first excited $2^+$ energy showing remarkable uniformity at ~1.2 MeV over a large range of neutron numbers [1]. Nevertheless, deformed states are also known to be part of the $Z$=50 and $Z$=51 landscape. Rotational bands with $\Delta I$=1 transitions have been observed in odd $_{51}$Sb nuclei [2], based on the high-$K$, $\beta$-upsloping $\pi g_{9/2}$ orbital intruding from below the $Z$=50 proton shell. Subsequently deformed states in even $_{50}$Sn nuclei were discovered via related decoupled $\Delta I$=2 rotational bands [3]. These states have a two-particle two-hole ($2p2h$) configuration $(\pi g_{7/2})^2\otimes(\pi g_{9/2})^{-2}$ with a prolate deformation regulated by the crossing of the $\pi g_{9/2}$ and $\pi g_{7/2}$ orbitals at $\beta_2 \sim 0.2$ [4]. More recently decoupled bands involving the low-$K$ prolate orbitals above the $Z$=50 proton shell have been found in odd-mass Sb nuclei. In $^{117}$Sb, three such structures are known which involve the three available proton orbitals $\pi d_{5/2}$, $\pi g_{7/2}$, and $\pi h_{11/2}$ coupled to the $2p2h$ deformed state in $^{116}$Sn [4]. A $\Delta I$=2 band has been found in $^{113}$Sb, which extends to high spin and high rotational frequency [5]. This band initiates from the $\pi h_{11/2}$ intruder orbital coupled

*Current address: Lawrence Livermore Laboratory, P.O. Box 808, Livermore, CA 94550.
†Current address: I.U.P.U.I., Indianapolis, IN 46202.
‡Current address: University of Tennessee, Knoxville, TN 37796; permanent address: Institute of Modern Physics, Lanzhou, People's Republic of China.
§Current address: Nuclear Science Division, Lawrence Berkeley Laboratory, Berkeley, CA 94720.
‖Current address: Centre de Recherches Nucléaires, 67037 Strasbourg Cedex, France.

 

to the $2p2h$ deformed $^{112}$Sn core. At high spins, alignments of additional nucleons have been observed in this band, with properties that are not well explained by the standard nuclear models. Recent results for $^{109}$Sb [6] and $^{106,108}$Sn [7,8] have revealed interesting rotational structures. These bands have dynamic moments of inertia which gradually decrease to very low values (approximately $\frac{1}{3}$ the rigid body value) at high rotational frequencies.

In order to explore the systematic properties of these structure features to more neutron-deficient nuclei, experiments have been performed to investigate $^{111}$Sb. Very little was known previously about the level scheme of this nucleus [9]. This investigation uncovered several interesting and unexpected features. Parts of this work resulting from the experiments performed at Stony Brook and Chalk River Laboratories have been previously reported [10].

## II. EXPERIMENTAL DETAILS

Three experiments were performed to populate a complete range of spins in $^{111}$Sb. Moderate-spin levels were studied using the FN tandem/Superconducting LINAC facility at Stony Brook. The reaction $^{96}$Ru($^{19}$F,$2p2n$)$^{111}$Sb was initiated with a 90-MeV $^{19}$F beam. The 1 mg/cm$^2$ target of enriched $^{96}$Ru was backed by $^{208}$Pb to stop the recoiling nuclei; this eliminated Doppler broadening of all but the fastest $\gamma$-ray transitions. An array of six Compton-suppressed Ge detectors was employed for the $\gamma$-ray measurement in conjunction with a 14-element BGO ball which subtended 80% of $4\pi$ solid angle, used as a multiplicity filter. A fold condition of two or more suppressed Ge signals in coincidence with two or more BGO elements was required for an event to be accepted. This reduced background from x-rays, Coulomb excitation, and other low-multiplicity events. Events meeting this criterion were then recorded onto magnetic tape; a total of $157\times10^6$ such events were recorded. These data were then sorted off-line into an $E_\gamma - E_\gamma$ matrix. Coincidence relationships determined from this matrix were used to construct the level scheme shown in Fig. 1. A sample coincidence spectrum showing band 5 from the backed target data is shown in Fig. 2.

Multipolarities of some $\gamma$ transitions were determined from directional correlation (DCO) analysis [11]. For this type of ratio analysis, detectors situated at 90° with respect to the beam direction are sorted against those at forward and backward angles. Transitions with known multipolarities in other nuclei populated in the reaction were used as a calibration. It was found that if the gate transition has a stretched $E2$ character, a DCO ratio of approximately 1.0 indicated a stretched quadrupole transition. A ratio of 0.50 was typical of a pure stretched dipole transition.

A second experiment, which used a self-supporting thin target, was performed using the TASCC (Tandem Accelerator Superconducting Cyclotron) facility at Chalk River Laboratories. In order to populate high-spin levels in $^{111}$Sb, a 120-MeV beam of $^{23}$Na was used to induce the $^{92}$Mo($^{23}$Na,$2p2n$)$^{111}$Sb reaction. The Chalk River $8\pi$ spectrometer, which consists of 20 Compton-suppressed Ge detectors and 71 inner-ball BGO elements, was employed to detect the emanating $\gamma$ rays. The target consisted of two stacked self-supporting foils, each with a thickness of 600 $\mu$g/cm$^2$. Doppler shifts of the $\gamma$ rays resulting from the recoil velocity of the residual nuclei were corrected on-line. A multiplicity requirement of two Ge detectors and eight or more BGO elements was required for an event to be written on magnetic tape. An analysis of the BGO ball average multiplicity ($K$) and total energy ($H$) per event for various reaction channels was then made to determine off-line parameter cuts. A multiplicity requirement of $K \geq 15$ was selected and no total energy cut was made; this requirement greatly enhanced the $2p2n$ reaction channel over other competing channels. Events meeting this requirement were sorted into an $E_\gamma - E_\gamma$ matrix, accumulating a total of $72\times10^6$ events.

A third experiment was performed at the 88-in. Cyclotron at Lawrence Berkeley Laboratories, with the Early Implementation of GAMMASPHERE. The reaction $^{54}$Fe($^{63}$Cu,$\alpha2p$) with a beam energy of 245 MeV populated $^{111}$Sb. The experiment was directed at the study of $^{114}$Te through the $3p$ channel, but the $\alpha2p$ channel proved to be populated with considerable strength. The target consisted of two self-supporting 500 $\mu$g/cm$^2$ foils of 97% isotopically pure $^{54}$Fe. At the time of the experiment, the GAMMASPHERE array consisted of 31 Compton-suppressed Ge detectors, each with an efficiency of approximately 75% of a standard 3 in. × 3 in. NaI at 1.3 MeV. Thirteen of these detectors were positioned at forward angles of less than 38° relative to the beam direction, and fifteen at backward angles all greater than 142°. The remaining three detectors were positioned at 90°. This forward-backward geometry minimized the effects of Doppler broadening; despite a high recoil velocity of 4.7% of $c$, the FWHM of peaks at 1 MeV was measured as only 6 keV after correcting for Doppler shifts. Only events in which three of these detectors registered a $\gamma$ ray were accepted and written onto magnetic tape. A total of $10^9$ such triples events were recorded. The triples data were then sorted off-line into an $E_\gamma - E_\gamma - E_\gamma$ cube. A sample of the thin-target data showing bands 2, 3, and 4 from GAMMASPHERE is shown in Fig. 3.

For all experiments, data analysis was greatly facilitated by the use of the programs GF2, ESCL8R, and LEVIT8R [12] written by D.C. Radford of Chalk River Laboratories.

## III. RESULTS

The proposed level scheme for $^{111}$Sb, derived from coincidence relationships and relative intensities, is shown in Fig. 1. Table I contains the transition energies, spin assignments, relative intensities, DCO ratios, and multipolarities assigned to the $\gamma$ rays identified in the backed-target experiment. Table II reports the energies, spin assignments, and relative intensities of the high-spin transi-

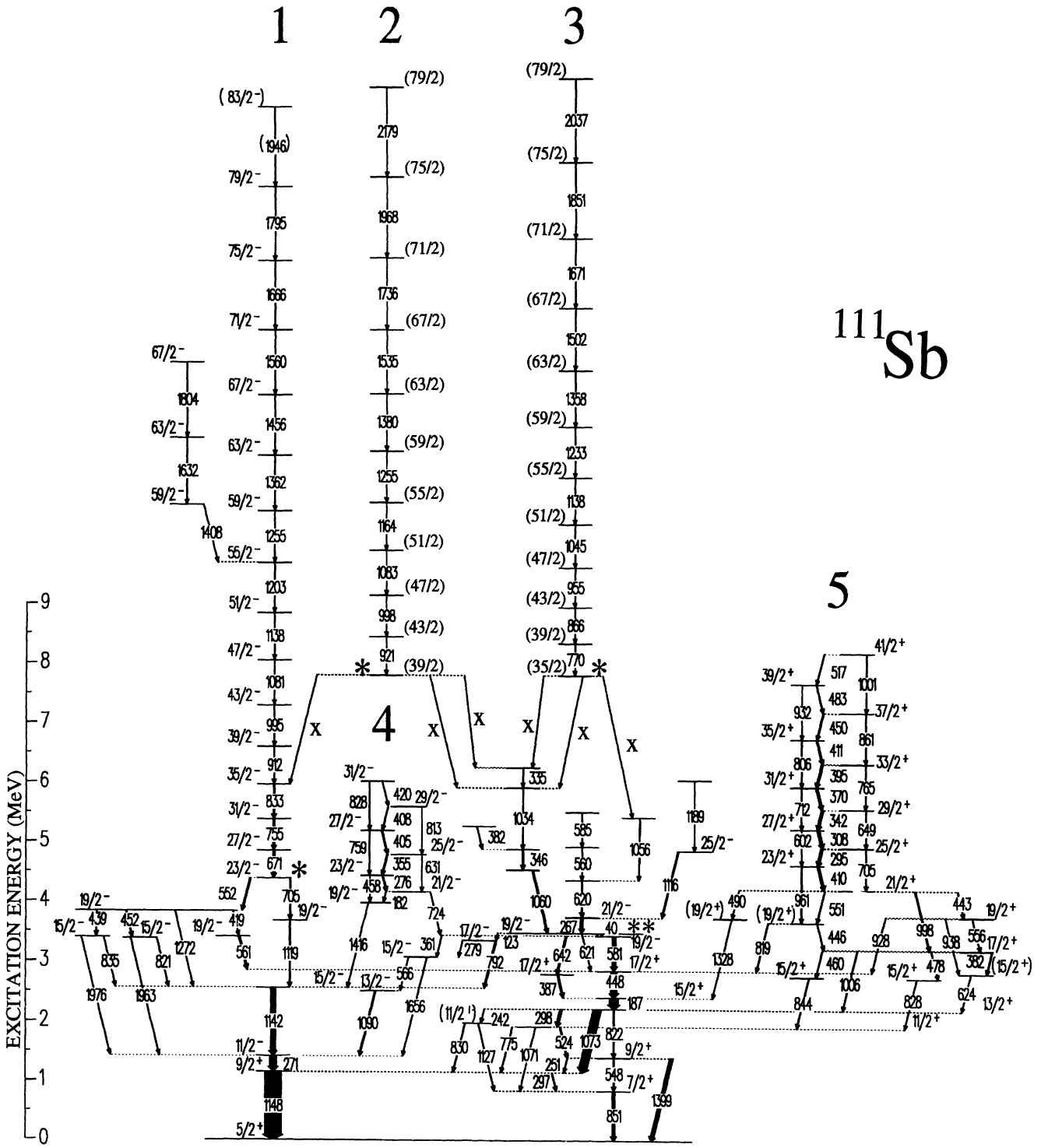


FIG. 1. The decay scheme of $^{111}$Sb deduced from this work. Gamma-ray energies are given in keV. The widths of the arrows represent the relative intensities of the transitions. For clarity the transitions in the three decoupled bands located above the levels marked with an asterisk are shown to a scale of 0.6; thus the energy scale shown at the left applies only to those levels which are not members of the decoupled bands. Transitions marked with an $X$ are intended only to indicate the decay patterns of the associated bands.

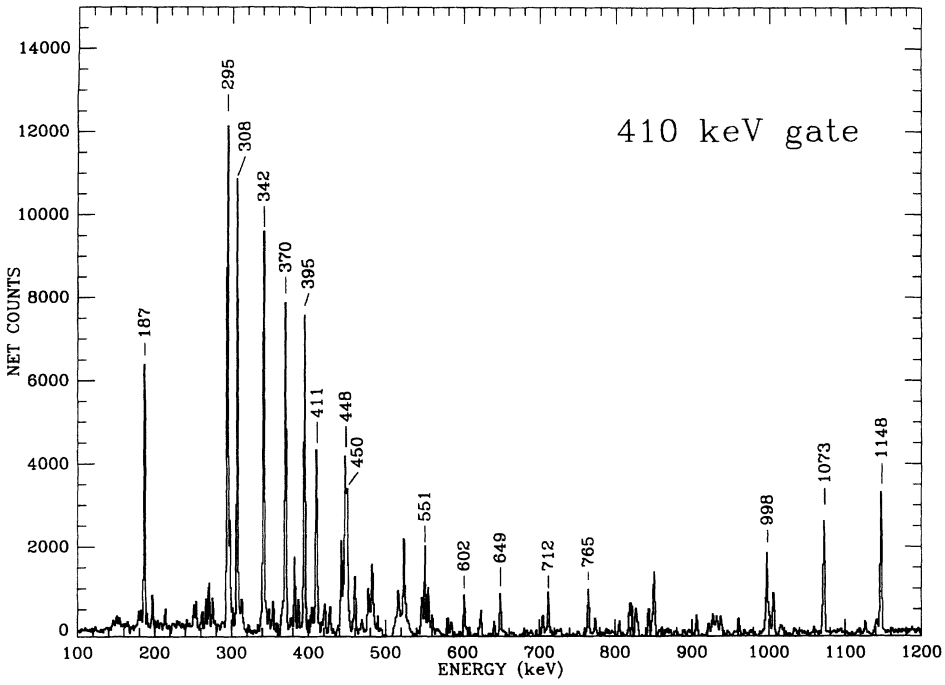


FIG. 2. A background subtracted coincidence spectrum from the backed-target experiment. The gated transition is at 410 keV and is a member of the proposed $(\pi g_{7/2})^2 \otimes (\pi g_{9/2})^{-1}$ band (band 5).

tions which were observed in the thin-target experiments. Spin assignments were made on the basis of DCO ratios and systematics. The ground state of $^{111}$Sb is assumed to have $I^\pi = \frac{5}{2}^+$ following the systematics of other odd Sb nuclei studied to date; beta-decay experiments support this assignment [13].

Figure 1 reveals a very complicated structure of single-particle levels as well as five rotational bands in $^{111}$Sb. Three of these bands are decoupled ($\Delta I$=2) and extend to rotational frequencies exceeding 1 MeV. These rotational bands can also be seen in Fig. 3. The remaining two bands are strongly coupled ($\Delta I$=1) bands. The decoupled band labeled 1, was populated with an intensity of approximately 20% of the $^{111}$Sb yield in both the Chalk River and GAMMASPHERE experiments, but only 10% in the Stony Brook experiment. It has been assigned a negative parity based on the proposed $E1$ assignment for the 271-keV transition connecting the $\frac{11}{2}^-$ and $\frac{9}{2}^+$ states. The DCO ratio measured for this transition was 0.45±0.03 which is consistent with a pure (no quadrupole mixing) stretched dipole assignment. Also, the $^{113,117,119}$Sb isotopes possess an $\frac{11}{2}^-$ state lying slightly above a $\frac{9}{2}^+$ state, with a low energy

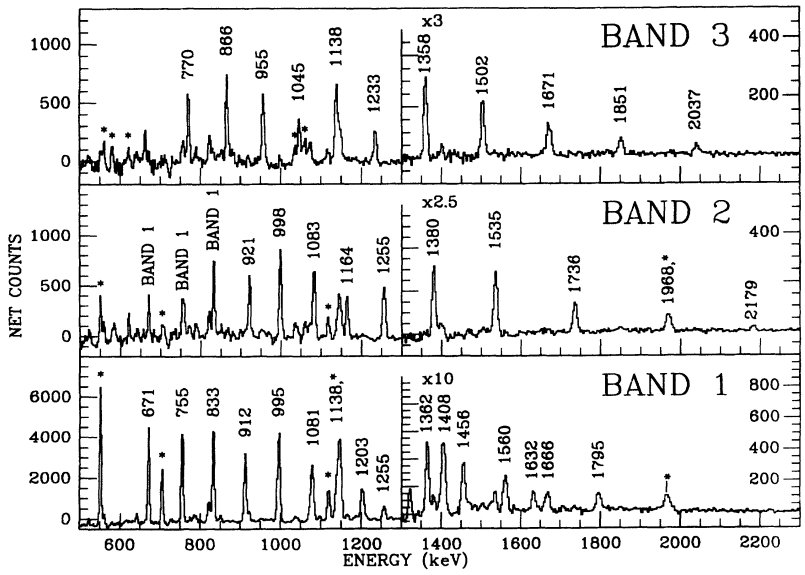


FIG. 3. Three spectra showing the decoupled bands found in $^{111}$Sb. The spectra were created by adding several double gates on the GAMMASPHERE $E_\gamma - E_\gamma - E_\gamma$ data. In all spectra, peaks representing transitions in the spherical part of the decay scheme are labeled with an asterisk; in the middle spectrum three peaks are labeled with BAND 1, showing the transitions in band 1 which are in coincidence with band 2. Note the change in scale of the $y$ axis in the spectra at 1300 keV.

TABLE I. Information on transitions assigned to $^{111}$Sb observed in the backed-target experiment.

| Energy, keV[a] | $I_i^\pi - I_f^\pi$ | Relative intensity[b] | DCO ratio[c] | Multipolarity |
|---|---|---|---|---|
| 123.4 | $\frac{19}{2}^- - \frac{17}{2}^-$ | <2 | 0.52±0.23 | $M1/E2$ |
| 182.1 | $\frac{21}{2}^- - \frac{19}{2}^-$ | <2 | 0.43±0.10 | $M1/E2$ |
| 186.6 | $\frac{15}{2}^+ - \frac{13}{2}^+$ | 48 | 0.39±0.02 | $M1/E2$ |
| 242.2 | $\frac{13}{2}^+ - (\frac{11}{2}^+)$ | <2 | [d] | $(M1/E2)$ |
| 251.1 | $\frac{9}{2}^+ - \frac{9}{2}^+$ | 2 | 0.42±0.14 | $M1/E2$ |
| 266.9 | $\frac{21}{2}^- - \frac{19}{2}^-$ | 14 | 0.31±0.31 | $M1/E2$ |
| 270.7 | $\frac{11}{2}^- - \frac{9}{2}^+$ | 38 | 0.45±0.03 | $E1$ |
| 275.5 | $\frac{23}{2}^- - \frac{21}{2}^-$ | 6 | 0.20±0.07 | $M1/E2$ |
| 278.5 | $\frac{17}{2}^- - \frac{15}{2}^-$ | <2 | [d] | $M1/E2$ |
| 294.9 | $\frac{25}{2}^+ - \frac{23}{2}^+$ | 13 | 0.62±0.11 | $M1/E2$ |
| 296.6 | $\frac{9}{2}^+ - \frac{7}{2}^+$ | 4 | [d] | $M1/E2$ |
| 298.1 | $\frac{13}{2}^+ - \frac{11}{2}^+$ | 14 | 0.60±0.09 | $M1/E2$ |
| 307.5 | $\frac{27}{2}^+ - \frac{25}{2}^+$ | 14 | 0.56±0.13 | $M1/E2$ |
| 334.6 | $\frac{31}{2}^- - \frac{29}{2}^-$ | <2 | [d] | $M1/E2$ |
| 341.9 | $\frac{29}{2}^+ - \frac{27}{2}^+$ | 13 | 0.61±0.07 | $M1/E2$ |
| 346.4 | $\frac{25}{2}^- - \frac{23}{2}^-$ | 6 | [d] | $M1/E2$ |
| 354.6 | $\frac{25}{2}^- - \frac{23}{2}^-$ | 6 | 0.54±0.24 | $M1/E2$ |
| 361.3 | $\frac{19}{2}^- - \frac{15}{2}^-$ | 2 | [d] | $E2$ |
| 370.4 | $\frac{31}{2}^+ - \frac{29}{2}^+$ | 11 | 0.45±0.08 | $M1/E2$ |
| 381.8 | $\frac{27}{2}^- - \frac{25}{2}^-$ | 2 | [d] | $M1/E2$ |
| 382.3 | $\frac{17}{2}^+ - (\frac{15}{2}^+)$ | 4 | [d] | $(M1/E2)$ |
| 387.0 | $\frac{17}{2}^+ - \frac{15}{2}^+$ | 8 | 0.53±0.11 | $M1/E2$ |
| 395.1 | $\frac{33}{2}^+ - \frac{31}{2}^+$ | 10 | 0.44±0.09 | $M1/E2$ |
| 404.5 | $\frac{27}{2}^- - \frac{25}{2}^-$ | 6 | [d] | $M1/E2$ |
| 408.3 | $\frac{29}{2}^- - \frac{27}{2}^-$ | 3 | [d] | $M1/E2$ |
| 410.0 | $\frac{23}{2}^+ - \frac{21}{2}^+$ | 12 | 0.41±0.16 | $M1/E2$ |
| 411.2 | $\frac{35}{2}^+ - \frac{33}{2}^+$ | 7 | 0.77±0.53 | $M1/E2$ |
| 418.5 | $\frac{19}{2}^- - \frac{19}{2}^-$ | <2 | 0.98±0.13 | $M1/E2$ |
| 420.2 | $\frac{31}{2}^- - \frac{29}{2}^-$ | 2 | [d] | $E2$ |
| 439.0 | $\frac{19}{2}^- - \frac{15}{2}^-$ | <2 | 1.12±0.40 | $E2$ |
| 442.6 | $\frac{21}{2}^+ - \frac{19}{2}^+$ | 3 | [d] | $M1/E2$ |
| 446.0 | $(\frac{19}{2}^+) - \frac{17}{2}^+$ | 2 | [d] | $(M1/E2)$ |
| 447.5 | $\frac{17}{2}^+ - \frac{15}{2}^+$ | 37 | 0.38±0.03 | $M1/E2$ |
| 450.0 | $\frac{37}{2}^+ - \frac{35}{2}^+$ | 5 | [d] | $M1/E2$ |
| 451.9 | $\frac{19}{2}^- - \frac{15}{2}^-$ | 3 | 1.01±0.32 | $E2$ |
| 457.7 | $\frac{23}{2}^- - \frac{19}{2}^-$ | <2 | [d] | $E2$ |
| 460.1 | $\frac{17}{2}^+ - \frac{15}{2}^+$ | 2 | 0.70±0.23 | $M1/E2$ |
| 477.7 | $\frac{17}{2}^+ - \frac{15}{2}^+$ | 2 | 0.87±0.53 | $M1/E2$ |
| 482.6 | $\frac{39}{2}^+ - \frac{37}{2}^+$ | 3 | [d] | $M1/E2$ |
| 489.8 | $\frac{21}{2}^+ - (\frac{19}{2}^+)$ | <2 | [d] | $(M1/E2)$ |
| 516.7 | $\frac{41}{2}^+ - \frac{39}{2}^+$ | 2 | [d] | $M1/E2$ |
| 523.7 | $\frac{11}{2}^+ - \frac{9}{2}^+$ | 5 | 0.95±0.13 | $M1/E2$ |
| 547.5 | $\frac{9}{2}^+ - \frac{7}{2}^+$ | 5 | 0.59±0.14 | $M1/E2$ |
| 551.2 | $\frac{21}{2}^+ - (\frac{19}{2}^+)$ | 3 | [d] | $(M1/E2)$ |
| 551.6 | $\frac{23}{2}^- - \frac{19}{2}^-$ | 7 | 1.04±0.09 | $E2$ |
| 555.5 | $\frac{19}{2}^+ - \frac{17}{2}^+$ | 2 | [d] | $M1/E2$ |
| 560.2 | $\frac{27}{2}^- - \frac{25}{2}^-$ | 2 | [d] | $M1/E2$ |
| 560.5 | $\frac{19}{2}^- - \frac{17}{2}^+$ | 9 | 0.43±0.08 | $E1$ |
| 565.5 | $\frac{15}{2}^- - \frac{13}{2}^-$ | <2 | [d] | $M1/E2$ |
| 581.0 | $\frac{19}{2}^- - \frac{17}{2}^+$ | 20 | 0.47±0.04 | $E1$ |
| 585.1 | $\frac{29}{2}^- - \frac{27}{2}^-$ | <2 | 0.55±0.24 | $M1/E2$ |
| 602.4 | $\frac{27}{2}^+ - \frac{23}{2}^+$ | <2 | [d] | $E2$ |
| 619.9 | $\frac{25}{2}^- - \frac{21}{2}^-$ | 6 | [d] | $E2$ |

TABLE I. *(Continued).*

| Energy, keV[a] | $I_i^\pi - I_f^\pi$ | Relative intensity[b] | DCO ratio[c] | Multipolarity |
|---|---|---|---|---|
| 621.1 | $\frac{19}{2}^- - \frac{17}{2}^+$ | 2 | [d] | $E1$ |
| 624.0 | $(\frac{15}{2}^+) - \frac{13}{2}^+$ | 2 | [d] | $(M1/E2)$ |
| 630.8 | $\frac{25}{2}^- - \frac{21}{2}^-$ | <2 | [d] | $E2$ |
| 641.6 | $\frac{19}{2}^- - \frac{17}{2}^+$ | 8 | 0.36±0.15 | $E1$ |
| 649.4 | $\frac{29}{2}^+ - \frac{25}{2}^+$ | 2 | [d] | $E2$ |
| 671.4 | $\frac{27}{2}^- - \frac{23}{2}^-$ | 11 | 0.95±0.11 | $E2$ |
| 704.8 | $\frac{25}{2}^+ - \frac{21}{2}^+$ | 2 | [d] | $E2$ |
| 704.9 | $\frac{23}{2}^- - \frac{19}{2}^-$ | 4 | 1.00±0.23 | $E2$ |
| 712.1 | $\frac{31}{2}^+ - \frac{27}{2}^+$ | 2 | [d] | $E2$ |
| 723.8 | $\frac{21}{2}^- - \frac{19}{2}^-$ | 2 | [d] | $M1/E2$ |
| 755.3 | $\frac{31}{2}^- - \frac{27}{2}^-$ | 10 | 0.95±0.07 | $E2$ |
| 758.8 | $\frac{27}{2}^- - \frac{23}{2}^-$ | <2 | [d] | $E2$ |
| 765.3 | $\frac{33}{2}^+ - \frac{29}{2}^+$ | 2 | [d] | $E2$ |
| 774.6 | $\frac{11}{2}^+ - \frac{9}{2}^+$ | 2 | 0.41±0.12 | $M1/E2$ |
| 791.6 | $\frac{17}{2}^- - \frac{15}{2}^-$ | 8 | 0.26±0.05 | $M1/E2$ |
| 805.9 | $\frac{35}{2}^+ - \frac{31}{2}^+$ | 2 | [d] | $E2$ |
| 812.6 | $\frac{29}{2}^- - \frac{25}{2}^-$ | <2 | [d] | $E2$ |
| 819.3 | $(\frac{19}{2}^+) - \frac{17}{2}^+$ | 3 | [d] | $(M1/E2)$ |
| 820.8 | $\frac{15}{2}^- - \frac{15}{2}^-$ | 2 | [d] | $M1/E2$ |
| 821.8 | $\frac{13}{2}^+ - \frac{9}{2}^+$ | 5 | 0.45±0.07 | $M1/E2$ |
| 827.5 | $\frac{15}{2}^+ - \frac{11}{2}^+$ | 2 | 1.25±0.70 | $E2$ |
| 827.9 | $\frac{31}{2}^- - \frac{27}{2}^-$ | <2 | [d] | $E2$ |
| 830.2 | $(\frac{11}{2}^+) - \frac{9}{2}^+$ | 3 | [d] | $(M1/E2)$ |
| 832.7 | $\frac{35}{2}^- - \frac{31}{2}^-$ | 8 | [d] | $E2$ |
| 834.9 | $\frac{15}{2}^- - \frac{15}{2}^-$ | <2 | [d] | $M1/E2$ |
| 844.1 | $\frac{15}{2}^+ - \frac{11}{2}^+$ | 3 | [d] | $E2$ |
| 851.1 | $\frac{7}{2}^+ - \frac{5}{2}^+$ | 16 | 0.22±0.06 | $M1/E2$ |
| 860.8 | $\frac{37}{2}^+ - \frac{33}{2}^+$ | <2 | [d] | $E2$ |
| 912.0 | $\frac{39}{2}^- - \frac{35}{2}^-$ | 4 | [d] | $E2$ |
| 927.7 | $\frac{19}{2}^+ - \frac{17}{2}^+$ | 2 | [d] | $M1/E2$ |
| 932.3 | $\frac{39}{2}^+ - \frac{35}{2}^+$ | <2 | [d] | $E2$ |
| 937.6 | $\frac{19}{2}^+ - \frac{15}{2}^+$ | <2 | [d] | $E2$ |
| 960.9 | $\frac{23}{2}^+ - (\frac{19}{2}^+)$ | 3 | [d] | $(E2)$ |
| 995.3 | $\frac{43}{2}^- - \frac{39}{2}^-$ | 2 | [d] | $E2$ |
| 997.6 | $\frac{21}{2}^+ - \frac{17}{2}^+$ | 6 | 1.12±0.65 | $E2$ |
| 1000.7 | $\frac{41}{2}^+ - \frac{37}{2}^+$ | <2 | [d] | $E2$ |
| 1006.2 | $\frac{17}{2}^+ - \frac{13}{2}^+$ | 3 | 1.97±0.66 | $E2$ |
| 1034.2 | $\frac{29}{2}^- - \frac{25}{2}^-$ | 4 | [d] | $E2$ |
| 1055.5 | $\frac{29}{2}^- - \frac{25}{2}^-$ | 3 | [d] | $E2$ |
| 1059.5 | $\frac{23}{2}^- - \frac{19}{2}^-$ | 8 | [d] | $E2$ |
| 1071.3 | $\frac{11}{2}^+ - \frac{7}{2}^+$ | <2 | [d] | $E2$ |
| 1072.5 | $\frac{13}{2}^+ - \frac{9}{2}^+$ | 48 | 1.02±0.06 | $E2$ |
| 1081.2 | $\frac{47}{2}^- - \frac{43}{2}^-$ | <2 | [d] | $E2$ |
| 1090.0 | $\frac{13}{2}^- - \frac{11}{2}^-$ | 6 | 0.50±0.41 | $M1/E2$ |
| 1116.4 | $\frac{25}{2}^- - \frac{21}{2}^-$ | 6 | 1.43±0.45 | $E2$ |
| 1118.8 | $\frac{19}{2}^- - \frac{15}{2}^-$ | 6 | 0.80±0.23 | $E2$ |
| 1126.8 | $(\frac{11}{2}^+) - \frac{7}{2}^+$ | 2 | [d] | $(E2)$ |
| 1142.3 | $\frac{15}{2}^- - \frac{11}{2}^-$ | 27 | 1.02±0.10 | $E2$ |
| 1147.6 | $\frac{9}{2}^+ - \frac{5}{2}^+$ | 100 | 1.04±0.10 | $E2$ |
| 1189.1 | $\frac{29}{2}^- - \frac{25}{2}^-$ | <2 | [d] | $E2$ |
| 1271.9 | $\frac{19}{2}^- - \frac{15}{2}^-$ | <2 | [d] | $E2$ |
| 1327.6 | $(\frac{19}{2}^+) - \frac{15}{2}^+$ | <2 | [d] | $(E2)$ |
| 1398.5 | $\frac{9}{2}^+ - \frac{5}{2}^+$ | 20 | 1.18±0.13 | $E2$ |

TABLE I *(Continued).*

| Energy, keV[a] | $I_i^\pi - I_f^\pi$ | Relative intensity[b] | DCO ratio[c] | Multipolarity |
|---|---|---|---|---|
| 1416.0 | $\frac{19}{2}^- - \frac{15}{2}^-$ | <2 | 1.03±0.45 | $E2$ |
| 1655.5 | $\frac{15}{2}^- - \frac{11}{2}^-$ | 2 | 1.15±0.47 | $E2$ |
| 1963.3 | $\frac{15}{2}^- - \frac{11}{2}^-$ | <2 | 0.99±0.34 | $E2$ |
| 1976.4 | $\frac{15}{2}^- - \frac{11}{2}^-$ | <2 | [d] | $E2$ |

[a]Transition energies accurate to within ±0.2 keV.
[b]Intensities are normalized to 100 for the 1147.6-keV transition.
[c]DCO ratios are from backed-target experiment only.
[d]Transition too weak to yield DCO ratio.

$E1$ transition connecting them [2]. (In $^{115}$Sb the $\frac{11}{2}^-$ state lies below the $\frac{9}{2}^+$ state and no connecting $E1$ transition is observed.) Band 1 in $^{111}$Sb has been observed up to $I^\pi=(\frac{83}{2}^-)$. The $\frac{11}{2}^-$ band member was not observed, as the band begins to decay out at a spin of $\frac{23}{2}^-$ into states which are presumably admixtures of single-particle and collective configurations. The majority of the decay out occurs via the $\frac{23}{2}^- - \frac{19}{2}^-$ 552-keV transition, the intensity then branches into four competing decay paths. The strongest decay path from this point is through the 452-keV $E2$ transition and then down through the spherical negative parity states. Finally, there is a short sequence of high energy, presumably $E2$ transitions feeding into band 1 at the $J^\pi=\frac{55}{2}^-$ level. This sequence was observed only in the GAMMASPHERE experiment, although the associated drop in the intensity of the in-band 1255-keV transition was seen in the Chalk River experiment.

The two other decoupled bands were weakly populated in the thin-target experiments, and were not observed in the backed target experiment. Band 2 was observed with a relative intensity of approximately 3% in the Chalk River experiment; band 3 was not observed. Bands 2 and 3 were each populated with an intensity of approximately 5% in the GAMMASPHERE experiment. Despite the high quality of the data and good statistics from the thin-target experiments, it was not possible to connect these two bands to either band 1, or to the spherical states of the level scheme. As Fig. 1 shows, band 2 appears to decay predominantly into band 1 at the $\frac{35}{2}^-$ state. It decays with less strength into two spherical states. Band 3 appears to decay into only spherical states and is not observed in coincidence with transitions from other bands. Since these two bands are not connected to the level scheme, it is not possible to assign them to a definite spin. However, it is possible to estimate the spins from a knowledge of the decay of these bands. Thus we have estimated the spins shown for these two bands by determining the highest spin state into which the bands decay. It is difficult to estimate the uncertainty in this determination, but it is likely $\sim 4\hbar$. It should also be noted that it is possible that the spins of these bands differ by only $1\hbar$ rather than $2\hbar$ as shown in the figure; this fact attains significance when we consider the quasiparticle interpretation of these structures.

Of the two strongly coupled bands, band 5 was populated with considerably more intensity than band 4. The $\Delta I=1$ mixed $M1/E2$ transitions are very intense compared with the $E2$ crossover transitions. Band 5, which decays out at the $\frac{21}{2}^+$ state, feeds into lower spin states via a number of decay paths. This band has been observed up to a spin of $I^\pi=\frac{41}{2}^+$. Band 4 has been assigned negative parity, based on the $E2$ character of the 1416-keV transition, determined through its DCO ratio. The 724-keV decay transition is too weak to extract a DCO ratio. A negative parity assignment is, however, consistent with the higher mass $^{115-119}$Sb nuclei, where negative parity $\Delta I=1$ bands have previously been observed [4,14]. There is evidence also for a similar strongly coupled negative parity band in $^{109}$Sb with weak $E2$ crossover transitions [6].

The 40-keV transition, linking two $\frac{19}{2}^-$ states was not observed in these experiments; its presence was inferred from coincidence intensity relationships among the 621-keV $\frac{19}{2}^- - \frac{17}{2}^+$, 123-keV $\frac{19}{2}^- - \frac{17}{2}^-$, 267-keV $\frac{21}{2}^- - \frac{19}{2}^-$, and 581-keV $\frac{19}{2}^- - \frac{17}{2}^+$ transitions. The existence of this strong low-energy transition also implies that the $\frac{19}{2}^-$ state at 3477 keV may have a lifetime of the order of nanoseconds. (This level is marked by a double asterisk in Fig. 1, and is fed by 1060-keV and 267-keV transitions. It is depopulated by the 40-keV and 123-keV transitions.) Indeed, a comparison between the backed and unbacked target data does suggest a lifetime for this state. The coincidence between the 581-keV and 267-keV transitions is strong in the backed-target experiment, but this is not the case in the two unbacked-target experiments, where the recoiling residual nuclei are free to recoil out of the detection region. A mean lifetime of the order of this recoil time, approximately 5 ns, would explain this coincidence difference.

## IV. DISCUSSION

### A. Proton orbitals coupled to $^{110}_{50}$Sn core spherical states

As Fig. 1 shows, a large number of single-particle levels have been identified in $^{111}$Sb as a result of this work,

extending in spin to over $\frac{25}{2}^-$. Several levels can be attributed to configurations involving the $^{110}$Sn ground state coupled to a single valence proton from outside the $Z$=50 closed shell. The ground state of $^{111}$Sb with $I^\pi=\frac{5}{2}^+$ results from the occupation of the $\pi d_{5/2}$ orbital. The $\frac{7}{2}^+$ state at 851 keV and the $\frac{11}{2}^-$ state at 1419 keV are attributed to the valence proton occupying the $\pi g_{7/2}$ and $\pi h_{11/2}$ orbitals, respectively.

TABLE II. Information on high-spin transitions observed in the thin target experiments.

| Energy, keV[a] | $I_i^\pi - I_f^\pi$ | Relative intensity[b] |
|---|---|---|
| 671.4 | $\frac{27}{2}^- - \frac{23}{2}^-$ | 100[c] |
| 755.3 | $\frac{31}{2}^- - \frac{27}{2}^-$ | 98[c] |
| 770.3 | $(\frac{39}{2}) - (\frac{35}{2})$ | 33[d] |
| 832.7 | $\frac{35}{2}^- - \frac{31}{2}^-$ | 95[c] |
| 865.7 | $(\frac{43}{2}) - (\frac{39}{2})$ | 27[d] |
| 912.0 | $\frac{39}{2}^- - \frac{35}{2}^-$ | 80[c] |
| 920.9 | $(\frac{43}{2}) - (\frac{39}{2})$ | 66[d] |
| 955.1 | $(\frac{47}{2}) - (\frac{43}{2})$ | 23[d] |
| 995.3 | $\frac{43}{2}^- - \frac{39}{2}^-$ | 76[c] |
| 998.1 | $(\frac{47}{2}) - (\frac{43}{2})$ | 55[d] |
| 1045.3(3) | $(\frac{51}{2}) - (\frac{47}{2})$ | 21[d] |
| 1081.2 | $\frac{47}{2}^- - \frac{43}{2}^-$ | 66[c] |
| 1082.9 | $(\frac{51}{2}) - (\frac{47}{2})$ | 45[d] |
| 1137.8 | $\frac{51}{2}^- - \frac{47}{2}^-$ | 48[c] |
| 1138.4(3) | $(\frac{55}{2}) - (\frac{51}{2})$ | 18[d] |
| 1164.1 | $(\frac{55}{2}) - (\frac{51}{2})$ | 40[d] |
| 1202.5 | $\frac{55}{2}^- - \frac{51}{2}^-$ | 35[c] |
| 1233.0(3) | $(\frac{59}{2}) - (\frac{55}{2})$ | 16[d] |
| 1254.7(3) | $\frac{59}{2}^- - \frac{55}{2}^-$ | 29[c] |
| 1255.2(3) | $(\frac{59}{2}) - (\frac{55}{2})$ | 33[d] |
| 1358.4(4) | $(\frac{63}{2}) - (\frac{59}{2})$ | 15[d] |
| 1362.3(4) | $\frac{63}{2}^- - \frac{59}{2}^-$ | 12[c] |
| 1380.1(3) | $(\frac{63}{2}) - (\frac{59}{2})$ | 27[d] |
| 1408.4 | $\frac{59}{2}^- - \frac{55}{2}^-$ | 14[d] |
| 1456.4(5) | $\frac{67}{2}^- - \frac{63}{2}^-$ | 6[c] |
| 1502.2(4) | $(\frac{67}{2}) - (\frac{63}{2})$ | 15[d] |
| 1535.4(4) | $(\frac{67}{2}) - (\frac{63}{2})$ | 18[d] |
| 1560.0(4) | $\frac{71}{2}^- - \frac{67}{2}^-$ | 3[c] |
| 1632.5(5) | $\frac{63}{2}^- - \frac{59}{2}^-$ | <2[d] |
| 1665.5(5) | $\frac{75}{2}^- - \frac{71}{2}^-$ | <2[c] |
| 1671.4(6) | $(\frac{71}{2}) - (\frac{67}{2})$ | 10[d] |
| 1736.3(6) | $(\frac{71}{2}) - (\frac{67}{2})$ | 12[d] |
| 1795(2) | $\frac{79}{2}^- - \frac{75}{2}^-$ | <2[c] |
| 1803.8(6) | $\frac{67}{2}^- - \frac{63}{2}^-$ | <2[d] |
| 1851.3(7) | $(\frac{75}{2}) - (\frac{71}{2})$ | 8[d] |
| 1946(4) | $(\frac{83}{2}^-) - \frac{79}{2}^-$ | <2[c] |
| 1968(1) | $(\frac{75}{2}) - (\frac{71}{2})$ | 6[d] |
| 2037(3) | $(\frac{79}{2}) - (\frac{75}{2})$ | <2[d] |
| 2179(2) | $(\frac{79}{2}) - (\frac{75}{2})$ | <2[d] |

[a]Transition energies accurate to within ±0.2 keV, except where noted in the table.
[b]Intensities are normalized to 100 for the 671.4-keV transition.
[c]Intensity reported is from the Chalk River experiment.
[d]Intensity reported is from the GAMMASPHERE experiment.

Several sequences of levels in $^{111}$Sb can be attributed to valence proton orbitals coupled to excited spherical states in the $^{110}$Sn core [15], principally the $0_1^+$-$2_1^+$-$4_1^+$ ground-state sequence. This core sequence coupled to the $\pi d_{5/2}$ orbital manifests itself as the $\frac{5}{2}^+$ ground state, the $\frac{9}{2}^+$ state at 1148 keV and the $\frac{13}{2}^+$ state at 2221 keV. The $\pi h_{11/2}$ orbital should also couple to this sequence of core states. The $\frac{15}{2}^-$ state at 2561 keV corresponds to the $\pi h_{11/2}$ orbital coupled to the $2_1^+$ state. It is difficult to associate a particular $\frac{19}{2}^-$ state with the $\pi h_{11/2} \otimes 4_1^+$ configuration because of the large number of $\frac{19}{2}^-$ states.

The even Sn nuclei also exhibit negative-parity spherical states. These states are attributed to two-quasineutron configurations involving a $\nu h_{11/2}$ neutron. The valence proton in $^{111}$Sb can couple to these states as well. In higher mass Sb isotopes, such states have been found to be isomeric [2,16]. Typically these isomers are composed of the valence proton occupying the $\pi g_{7/2}$ or $\pi d_{5/2}$ orbital coupled to either the $5^-$ or $7^-$ states from the Sn core. The $\frac{19}{2}^-$ state which shows evidence of a lifetime in $^{111}$Sb may have such a configuration.

## B. Proton orbitals coupled to deformed states in $^{110}$Sn

### 1. Band 1

One of the striking features of the $^{111}$Sb level scheme is the long sequence of high energy transitions labeled band 1 on the left side of Fig. 1, which starts from an excitation energy of 4.385 MeV and $I^\pi=\frac{23}{2}^-$ and extends to 23 MeV and $I^\pi=(\frac{83}{2}^-)$. The nearly constant energy spacings between the peaks in this spectrum are indicative of a rotational band, with the top transitions implying a rotational frequency of $\hbar\omega$=0.97 MeV. DCO ratios have been measured for the lower-lying transitions, revealing a stretched quadrupole character. No signature partner to this band was observed in this experiment, which indicates a large signature splitting. Such a large signature splitting is the hallmark of a low-$K$ configuration, $K$ being the projection of the angular momentum on the symmetry axis of the nucleus. Of the low-$K$ orbitals that are nearest the Fermi surface, the $\pi h_{11/2}(\Omega=\frac{1}{2})$ quasiparticle is the most likely candidate. This orbital is deformation driving and is also consistent with the proposed negative parity of the band. However, the presence of a *spherical* state at 1419 keV built on this orbital suggests that this orbital alone cannot account for the deformation implied by this rotational structure. Therefore it is expected that this rotational band is based on the $h_{11/2}$ proton being coupled to the $2p2h$ deformed band of the $^{110}$Sn core. The deformed $[(\pi g_{9/2})^{-2} \otimes (\pi g_{7/2})^2]_{0^+}$ configuration is the basis of the positive parity rotational bands observed in the even Sn nuclei from $^{106}$Sn to $^{118}$Sn [3,7,8]. It is thus proposed that band 1 in $^{111}$Sb is based on the configuration $\pi h_{11/2} \otimes [(\pi g_{7/2})^2 \otimes (\pi g_{9/2})^{-2}]_{0^+}$.

This feature of the valence proton being coupled to both spherical and deformed core states has been observed previously in the $^{113-119}$Sb isotopes [4,5,14]. In $^{117}$Sb for example [4], spherical states with $I^\pi=\frac{5}{2}^+$, $\frac{7}{2}^+$, and $\frac{11}{2}^-$ have been observed and attributed to the occupation of the $\pi d_{5/2}$, $\pi g_{7/2}$, and $\pi h_{11/2}$ orbitals, respectively, coupled to the spherical core ground state. These same orbitals were also found to couple to the $2p2h$ deformed band of the $^{116}$Sn core, yielding three decoupled rotational bands. In $^{113}$Sb a single rotational band based on the $\pi h_{11/2}$ orbital coupled to the $2p2h$ core is observed, as well as the corresponding spherical $\frac{11}{2}^-$ state [5].

The rotational band in $^{111}$Sb was not observed down to the $\frac{11}{2}^-$ band member in the present experiments; at $I^\pi=\frac{23}{2}^-$ the band begins to decay out through a large number of competing decay paths. This is a common feature of the low-lying decoupled bands discovered in even Sn and odd Sb nuclei [3–5] as the lower spin rotational levels admix with spherical states having comparable excitation energies. In $^{117}$Sb, the $\pi h_{11/2}$ band is observed down to the $\frac{19}{2}^-$ state, where it then decays into two $\frac{15}{2}^-$ states. These $\frac{15}{2}^-$ states, which are possibly admixed, correspond to the $\pi h_{11/2}$ orbital coupled to the deformed and spherical $2^+$ states of the $^{116}$Sn core. The two other decoupled bands found in $^{117}$Sb decay in a similar manner. In $^{111}$Sb, the band decays into two admixed $I^\pi=\frac{19}{2}^-$ states involving the $\pi h_{11/2}$ orbital coupled to the deformed and spherical $4^+$ core states.

Total Routhian surface (TRS) calculations [17] which minimize the energy of the nucleus in the rotating frame with respect to the deformation parameters $\beta_2$, $\beta_4$, and $\gamma$ add credence to this interpretation of band 1 in $^{111}$Sb. Energy surfaces for the lowest proton configuration of negative signature and parity are shown in Fig. 4 for two frequencies. A distinct minimum is seen in these plots with a deformation of $\beta_2=0.24$ and a near-zero value of the triaxiality parameter $\gamma$, indicating a deformed prolate shape.

Figure 5 shows plots of the dynamic moment of inertia ($\mathcal{J}^{(2)}$) and relative alignment extracted from band 1 in $^{111}$Sb, and for the $\pi h_{11/2}$ band in $^{113}$Sb [5]. The $\mathcal{J}^{(2)}$ is defined by the expression $\hbar dI/d\omega$, and the rotational frequency $\hbar\omega$ is given by $dE/dI$. The relative alignment is defined as $i_x = I_x(\omega) - \mathcal{J}_0\omega/\hbar$; a value of $\mathcal{J}_0=23\hbar^2$/MeV was employed [5]. In calculating the $\mathcal{J}^{(2)}$ values for band 1 in $^{111}$Sb it was assumed that the 552-keV $\frac{23}{2}^-$-$\frac{19}{2}^-$ and 452-keV $\frac{19}{2}^-$-$\frac{15}{2}^-$ transitions were band members. From these plots, the rotational frequencies at which the angular momenta of pairs of quasiparticles align along the axis of rotation can be determined. Two such alignments can be seen for band 1 in $^{111}$Sb in Fig. 5. The first occurs at a rotational frequency $\hbar\omega$ ~0.42 MeV. This can be observed as a broad peak in the $\mathcal{J}^{(2)}$ plot around this frequency. The second alignment which can be seen in Fig. 5 occurs at a rotational frequency of $\hbar\omega$ ~0.6 MeV. It is difficult to distinguish between the two crossings in the plot of the relative alignment. However, it can be noted that the total gain in the relative alignment is approximately $15\hbar$.

Cranked Woods-Saxon calculations using the deformation parameters extracted from the TRS calculations have been used to interpret these crossings. These calculations predict an $h_{11/2}$ neutron crossing to occur at $\hbar\omega$=0.35 MeV, and a $g_{7/2}$ proton crossing at $\hbar\omega$=0.6 MeV. No other crossings are expected theoretically in the frequency range $\hbar\omega$ <0.6 MeV. Thus, the first experimental crossing is identified with the breaking of a pair of $h_{11/2}$ neutrons, and the second interpreted as the $\pi g_{7/2}$ alignment. These two processes can yield, at most, a total of $16\hbar$ gain in the relative alignment; thus these assignments are consistent with the experimentally measured gain in the relative alignment. This interpretation of the two alignments observed in this band in $^{111}$Sb is also consistent with what has been reported in $^{113}$Sb [5].

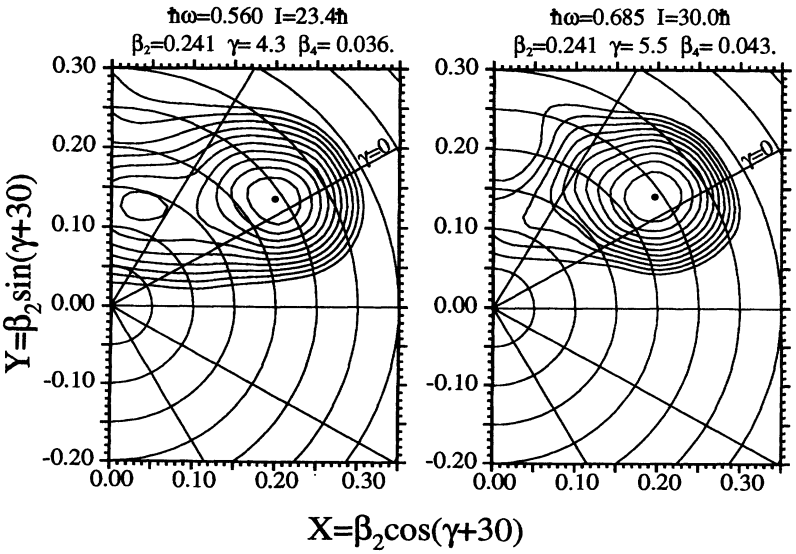


FIG. 4. TRS calculations showing the deformed minimum associated with the $\pi h_{11/2}$ proton for frequencies of $\hbar\omega$=0.560 MeV and 0.685 MeV, near the proposed $\pi g_{7/2}$ pair alignment.

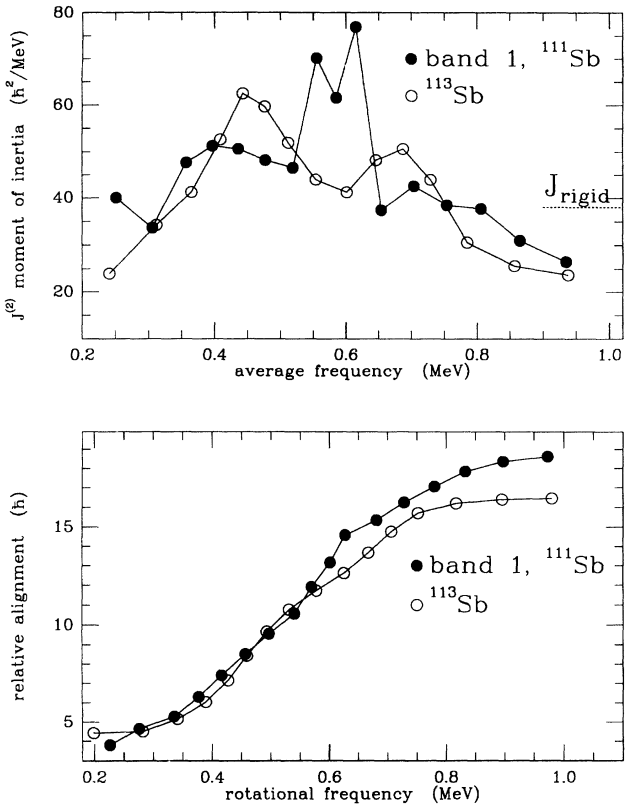


FIG. 5. Plots of the dynamic moment of inertia $\mathcal{J}^{(2)}$ and relative alignment for band 1 in $^{111}$Sb, and for the $\pi h_{11/2}$ band observed in $^{113}$Sb [5]. Solid circles represent $^{111}$Sb and open circles represent $^{113}$Sb. In calculating the relative alignment for $^{111}$Sb, a value of $\mathcal{J}_0$=23$\hbar^2$/MeV was used for the Harris parametrization.

It should be noted however that while the cranked Woods-Saxon calculation correctly predicts the experimental crossing frequency of the $\pi g_{7/2}$ crossing, it appears experimentally that the neutron $h_{11/2}$ crossing is delayed in frequency by approximately 0.07 MeV. Satuła *et al.* [18] have calculated the effect of a quadrupole-quadrupole neutron-proton interaction on the crossing frequencies. They suggest that a sizable interaction can occur in odd-proton nuclei when (i) the proton Fermi level is below the orbital occupied by the odd particle and (ii) the occupied orbital has a quadrupole moment substantially different from the average value. Both conditions are well satisfied in the $\pi h_{11/2}$ intruder bands in odd Sb nuclei. The calculations predict that the crossing frequencies should be higher in the Sb $\pi h_{11/2}$ bands than in the Sn-core bands, by 0.02-to-0.03 MeV/$\hbar$ compared with observed shifts of 0.09 MeV/$\hbar$ ($^{113}$Sb) and $\sim$ 0.03 MeV/$\hbar$ ($^{111}$Sb), relative to the crossing in the Sn core bands. Thus for the most part, the calculated effects of a quadrupole-quadrupole neutron-proton residual interaction are smaller than observed.

The fact that the two crossings can be distinguished from each other in the $\mathcal{J}^{(2)}$ plot allows for the extraction of the experimental interaction strength in the manner described in Ref. [5]. The interaction strength can be obtained from the dynamic moment of inertia, by

$$V_{\rm int} = \frac{\Delta i^2/4}{\left(\mathcal{J}^{(2)}_{\rm max} - \mathcal{J}^{(2)}_0\right)} \quad (1)$$

and

$$\Delta i = \int (\mathcal{J}^{(2)} - \mathcal{J}^{(2)}_0) d\omega \quad (2)$$

where $\mathcal{J}^{(2)}_0$ and $\mathcal{J}^{(2)}_{\rm max}$ are the unperturbed and maximum value of the $\mathcal{J}^{(2)}$ moment of inertia, respectively. This assumes a constant moment of inertia for the underlying core, and an interaction which is spin and frequency independent. Unlike $^{113}$Sb, accurate values of $\mathcal{J}^{(2)}_0$ and $\Delta i$ cannot be obtained in $^{111}$Sb, because of the irregularity in the $\mathcal{J}^{(2)}$ plot at the lowest frequency. If the $^{113}$Sb values of Ref. [5] are used, namely, $\mathcal{J}^{(2)}_0$=23$\hbar^2$MeV$^{-1}$ and $\Delta i$=7.3$\hbar$, an interaction strength of 470 keV is obtained for $^{111}$Sb. The value extracted for the same crossing in $^{110}$Sn cannot be measured accurately either, since the band is not observed below the $10^+$ level [15]. Assuming the peak in the $\mathcal{J}^{(2)}$ is observed, and using the same $\mathcal{J}^{(2)}_0$ and $\Delta i$ values as earlier, we find the experimental interaction strength of the $^{110}$Sn core to be 160 keV, indicating a $\sim$ 300 keV difference between the two interaction strengths. This difference is identical to that extracted for $^{113}$Sb, suggesting that the proposed residual interaction between valence $h_{11/2}$ neutrons and protons is similar in the two cases. The calculations by Satuła *et al.* [18] predict this difference in interaction strengths to be 60 keV, again significantly less than experimentally observed.

Finally, the $\mathcal{J}^{(2)}$ plot for band 1 shows an irregularity at approximately $\hbar\omega$=0.60 MeV. This irregularity results from the presence of the short sequence which feeds into band 1 at the $\frac{55}{2}^-$ state. The $\frac{59}{2}^-$ states in band 1 and in the side-band interact and repel each other. The resulting change in the transition energies of the $\gamma$ rays depopulating these levels causes the $\mathcal{J}^{(2)}$ values to shift. Three successive values of the $\mathcal{J}^{(2)}$ are affected as follows: the first $\mathcal{J}^{(2)}$ value is shifted upward, the second downward and the third upward. These shifts begin in Fig. 6 at a rotational frequency slightly greater than $\hbar\omega$=0.6 MeV.

### 2. *Bands 2 and 3*

The lack of definite spin assignments for bands 2 and 3 makes interpretations difficult. However, two bands with similar dynamic moments of inertia have been observed in $^{109}$Sb [6]. Thus it seems likely that bands 2 and 3 in $^{111}$Sb possess interpretations similar to the two bands observed in $^{109}$Sb. In Ref. [6] two possible interpretations for these two bands in $^{109}$Sb were given. The first involves a broken pair of neutrons $\nu g_{7/2}\nu h_{11/2}$ coupled to the configuration of band 1 in $^{111}$Sb, $\pi h_{11/2} \otimes (\pi g_{7/2})^2 \otimes (\pi g_{9/2})^{-2}$. The two bands would be signature partners in this scenario. In this configuration an $h_{11/2}$ neutron alignment would be blocked, and a $\pi g_{7/2}$ alignment would be expected to occur at

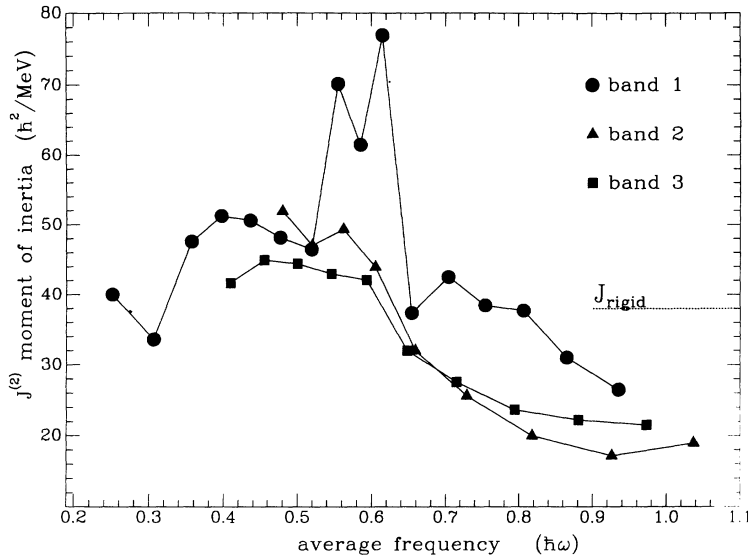


FIG. 6. Plots of the dynamic moment of inertia $\mathcal{J}^{(2)}$ for the three decoupled rotational bands identified in this work. The dotted line shows the value of the rigid body estimate of the moment of inertia, calculated for a deformation of $\beta_2=0.2$.

approximately $\hbar\omega=0.6$ MeV; the $\mathcal{J}^{(2)}$ of the two bands in $^{111}$Sb does not show clear evidence for such an alignment. However, TRS calculations do predict a strongly deformed prolate shape for such a configuration at the estimated empirical spin values.

The alternative explanation put forward in Ref. [6] for the bands in $^{109}$Sb involves a variant of the $2p2h$ core structure. One of the protons occupying the $g_{7/2}$ orbital is promoted to the $h_{11/2}$ orbital. Again, the two bands would be signature partners. This configuration blocks the $\pi g_{7/2}$ crossing, but does not block the neutron $h_{11/2}$ crossing at $\hbar\omega=0.35$ MeV. The $\mathcal{J}^{(2)}$ for bands 2 and 3 in $^{111}$Sb do not show definitive evidence for the neutron $h_{11/2}$ alignment, but the initial high value of the $\mathcal{J}^{(2)}$ is suggestive of such an alignment. It is also possible that rather than being signature partners of the same configuration, bands 2 and 3 in $^{111}$Sb may be interpreted as each possessing one of the discussed configurations.

At the highest rotational frequencies, near 1 MeV, it can be seen in Fig. 6 that the $\mathcal{J}^{(2)}$ decreases steadily to low values; in bands 2 and 3 the $\mathcal{J}^{(2)}$ decreases to values of approximately $20\hbar^2$/MeV. This characteristic, namely, slowly decreasing moments of inertia at high rotational frequencies, is consistent with the properties of rotational bands found in $^{109}$Sb [6], $^{106,108}$Sn [7,8], and also in $^{82}$Sr [19]. The lack of expected quasiparticle alignments in this high frequency region has been attributed to a loss of static pairing correlations [6,19]. Also, the slow decrease in the value of the $\mathcal{J}^{(2)}$ is evidence for a novel type of band termination [6,20]. Band termination in this mass region has been previously observed in several $_{53}$I [21], and $_{54}$Xe [22] isotopes. Typically this type of band termination is manifest as an abrupt end of the rotational sequence when the band is crossed by an aligned configuration with a noncollective oblate shape (single-particle structure). Generally the terminating bands are very irregular sequences, the irregularities likely being the result of mixing between the rotational and noncollective states. The rotational bands in $^{111}$Sb are very regular sequences. Rather than being crossed by a different noncollective configuration, the band retains the initial quasiparticle basis until the point where the spin that can be contributed by the valence particles is exhausted. As the angular momenta of the valence particles slowly align with the rotational axis, a gradual change in the nuclear shape from collective prolate to noncollective oblate occurs. The gradual loss of collectivity makes additional units of spin more costly, steadily increasing the in-band $E2$ transition energies. This slow increase reveals the observed slow decrease of the $\mathcal{J}^{(2)}$ values. Eventually the spin contributed by the valence particles is exhausted and the band terminates. For the configuration assigned to band 1, the terminating state is expected to have $J^\pi=\frac{95}{2}^-$; the terminating spin results from a fully aligned $(\nu h_{11/2})^4(\nu g_{7/2})^4(\nu d_{5/2})^2\otimes(\pi g_{9/2})^{-2}(\pi g_{7/2})^2(\pi h_{11/2})$ configuration. The terminating states for the proposed configurations of bands 2 and 3 should have nearly the same spins. Thus the final terminating states have most likely not been observed in these experiments.

### 3. *Bands 4 and 5*

Two other rotational structures have been extracted from the data. Band 5 was observed with considerable intensity. A sequence of ten transitions was found to be mutually coincident and determined to be predominantly dipole in character through the DCO ratios. Crossover transitions, which were observed with DCO ratios consistent with a stretched $E2$ character, represent the two signatures of the rotational band. A comparison of the Routhians of the two signatures shows that the $E2$ sequences have a very small signature splitting. This is similar to other strongly coupled bands found in higher odd-mass Sb, I ($Z=53$) and Cs ($Z=55$) nuclei [4,23,24]. The proposed quasiparticle configuration for this band is $(\pi g_{7/2})^2\otimes(\pi g_{9/2})^{-1}$. This configuration has $K=\frac{9}{2}$, which

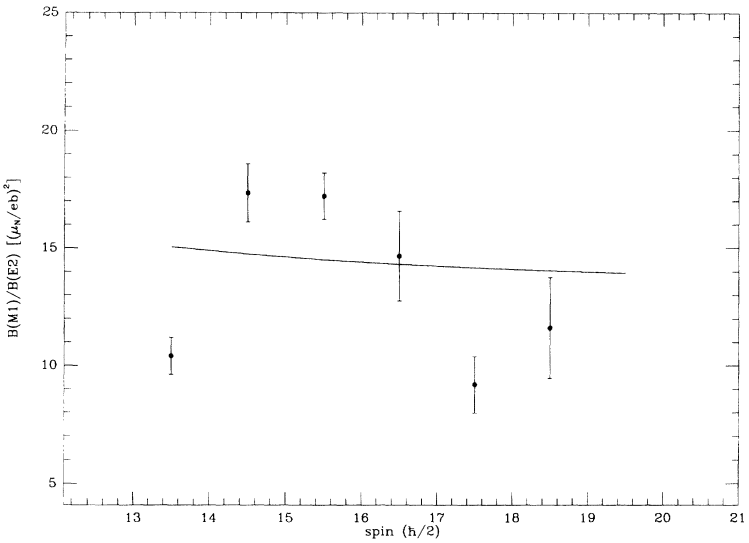


FIG. 7. Plot of experimental and theoretical B($M1;I \rightarrow I\text{-}1$)/B($E2;I \rightarrow I\text{-}2$) ratios of reduced transition probabilities extracted for band 5. The semiclassical prescription of Dönau and Frauendorf [25] was used to calculate the theoretical values.

explains the lack of signature splitting in this band. The B($M1;I \rightarrow I\text{-}1$)/B($E2;I \rightarrow I\text{-}2$) ratios extracted for this band (the small and positive [2] mixing ratios $\delta_{E2/M1}$ were neglected) are shown in Fig. 7, together with predicted values calculated with the semiclassical prescription of Dönau and Frauendorf [25]. It is seen that for the majority of this band, the experimental ratios are large, as is obvious from the intense $\Delta I=1$ transitions; this is consistent with the $K^2$ dependence ($K=\frac{9}{2}$) of the calculated values.

There is one significant difference between this band in $^{111}$Sb and the $(\pi g_{7/2})^2 \otimes (\pi g_{9/2})^{-1}$ proton two-particle one-hole ($2p1h$) bands observed in higher mass Sb nuclei. In $^{111}$Sb, this proton $2p1h$ strongly coupled band is not observed down to the $\frac{9}{2}^+$ band member, but instead decays out at the $I^\pi=\frac{21}{2}^+$ member. The complicated decay proceeds primarily through the $\frac{9}{2}^+$ state at 1.399 MeV. This change in the decay process can be attributed to the decreased deformation of the $(\pi g_{7/2})^2 \otimes (\pi g_{9/2})^{-1}$ bandhead in $^{111}$Sb compared with the heavier mass Sb nuclei. Table III shows the results of potential energy surface calculations for the $(\pi g_{7/2})^2 \otimes (\pi g_{9/2})^{-1}$ bandhead for a series of odd Sb nuclei; the deformation decreases steadily as the neutron number decreases. In addition, the potential minimum is broader in the lesser deformed nuclei, which allows for more vibrational-like levels to couple to the proton $2p1h$ state and admix with the rotational states. This may explain why the band decays into such a complicated group of levels, rather than directly to the $\frac{9}{2}^+$ state. Only at higher rotational frequencies where the band has become more deformed do the rotational levels dominate and become yrast. In the case of $^{111}$Sb this occurs at $I^\pi=\frac{21}{2}^+$.

TABLE III. The deformation of the $(\pi g_{7/2})^2 \otimes (\pi g_{9/2})^{-1}$ bandhead predicted by potential energy surface calculations for neutron numbers 58–68.

| Neutron number | $\beta_2$ |
|---|---|
| 58 | 0.167 |
| 60 | 0.172 |
| 62 | 0.194 |
| 64 | 0.211 |
| 66 | 0.222 |
| 68 | 0.206 |

Band 4 is another strongly coupled band. A strong sequence of $\Delta I=1$ mixed $M1/E2$ transitions is observed with weak $E2$ crossover transitions. No signature splitting is observed in this band. DCO ratios of transitions decaying out of this band suggest a negative-parity assignment. Negative-parity strongly coupled bands have been previously reported in other odd-mass Sb nuclei [4,26]. For example, in $^{117}$Sb, a strongly coupled band is built on a known isomer, the $g$ factor of which has been measured [16]. This measurement is consistent with the quasiparticle assignment $(\pi g_{7/2})^2 \otimes (\pi g_{9/2})^{-1} \otimes 7^-$ for the isomer, where the $7^-$ refers to the two-neutron state of the Sn core. A quadrupole moment measurement showed that this state was indeed deformed, having a deformation of $\beta=0.24$ [16]. It is suggested that band 4 in $^{111}$Sb results from the same configuration.

## V. CONCLUSIONS

In summary, high-spin states in the nucleus $^{111}$Sb, having one proton outside the $Z=50$ closed proton Sn shell, have been extensively studied for the first time. This nucleus has been shown to possess a variety of deformed and spherical states, which result from the coupling of the valence proton to both deformed and spherical states of the $^{110}_{50}$Sn core. Many spherical states in $^{111}$Sb are the result of the valence proton coupling to the near-spherical ground state sequence of the $^{110}_{50}$Sn core. A decoupled ($\Delta I=2$) rotational band has been found to involve the $\pi h_{11/2}$ valence proton orbital coupled to a $2p2h$ deformed sequence of the $^{110}$Sn core. Quasiparticle alignments and interaction strengths have been extracted for

this band. The $\nu h_{11/2}$ crossing frequency and the interaction strength are shown to deviate from the Cranked Woods-Saxon model predictions. Two other decoupled rotational bands were also observed. All three decoupled bands are observed to a high rotational frequency (up to 1.0 MeV) with decreasing moments of inertia. The smooth decrease of the dynamic moments of inertia of these bands at the highest rotational frequencies has been interpreted as a new form of gradual band termination. Also, two strongly coupled rotational bands involving the $(\pi g_{9/2})^{-1}$ orbital have been identified, one of which involves the coupling of this structure to a two-neutron negative-parity state of the $^{110}$Sn core.

## ACKNOWLEDGMENTS

Our thanks to R. Wyss for supplying the mesh used in the TRS calculations. In particular we appreciate the assistance of A.O. Macchiavelli and I.Y. Lee regarding the initial set-up procedures for GAMMASPHERE. We also wish to thank the staffs of the Stony Brook, TASCC and LBL facilities for the beams and targets. This work was supported in part by the National Science Foundation, AECL Research, Canadian NSERC, UK SERC, and NATO, under Grant No. CRG 910182. One of us (J.-y.Z.) would like to acknowledge NSF Grant No. INT-9001476. R.M.C. and S.A.F. acknowledge receipt of SERC postgraduate studentships.

[1] *Tables of Isotopes*, 7th edition, edited by C.M. Lederer and V.S. Shirley (Wiley, New York, 1978).

[2] A.K. Gaigalas, R.E. Shroy, G. Schatz, and D.B. Fossan, Phys. Rev. Lett. **35**, 555 (1975); Phys. Rev. C **19**, 1324 (1979).

[3] J. Bron, W.H.A. Hesselink, A. Van Poelgeest, J.J.A. Zalmstra, M.J. Uitzinger, and H. Verheul, Nucl. Phys. **A318**, 335 (1979).

[4] D.R. LaFosse, D.B. Fossan, J.R. Hughes, Y. Liang, P. Vaska, M.P. Waring, and J.-y. Zhang, Phys. Rev. Lett. **69**, 1332 (1992).

[5] V.P. Janzen, H.R. Andrews, B. Haas, D.C. Radford, D. Ward, A. Omar, D. Prévost, M. Sawicki, P. Unrau, J.C. Waddington, T.E. Drake, A. Galindo-Uribarri, and R. Wyss, Phys. Rev. Lett. **70**, 1065 (1993).

[6] V.P. Janzen, D.R. LaFosse, H. Schnare, D.B. Fossan, A. Galindo-Uribarri, J.R. Hughes, S.M. Mullins, E.S. Paul, L. Persson, S. Pilotte, D.C. Radford, I. Ragnarsson, P. Vaska, J.C. Waddington, R. Wadsworth, D. Ward, J. Wilson, and R. Wyss, Phys. Rev. Lett. **72**, 1160 (1994).

[7] R. Wadsworth, H.R. Andrews, C.W. Beausang, R.M. Clark, J. DeGraaf, D.B. Fossan, A. Galindo-Uribarri, I.M. Hibbert, K. Hauschild, J.R. Hughes, V.P. Janzen, D.R. LaFosse, S.M. Mullins, E.S. Paul, L. Persson, S. Pilotte, D.C. Radford, H. Schnare, P. Vaska, D. Ward, J.N. Wilson, and I. Ragnarsson, Phys. Rev. C **50**, 483 (1994).

[8] R. Wadsworth, H.R. Andrews, R.M. Clark, D.B. Fossan, A. Galindo-Uribarri, J.R. Hughes, V.P. Janzen, D.R. LaFosse, S.M. Mullins, E.S. Paul, D.C. Radford, H. Schnare, P. Vaska, D. Ward, J.N. Wilson, and R. Wyss, Nucl. Phys. **A559**, 461 (1993).

[9] V.E. Iacob, C. Stan-Sion, A. Berinde, I. Neamu, M. Parlog, N. Scintei, and L. Trache, Z. Phys. **A329**, 381 (1988).

[10] D.R. LaFosse, D.B. Fossan, P. Vaska, M.P. Waring, V.P. Janzen, S. Mullins, S. Pilotte, D.C. Radford, D. Ward, E.S. Paul, and R. Wadsworth, Bull. Am. Phys. Soc. **38**, 980 (1993).

[11] K.S. Krane, R.M. Steffen, and R.M. Wheeler, Nucl. Data Tables **A11**, 351 (1973).

[12] D.C. Radford, *Workshop on Large Gamma-Ray Detector Arrays*, Chalk River Laboratories, Canada, 1992 [AECL Report No. 10613, 1992 (unpublished)], Vol. 2, p. 403.

[13] M.E.J. Wigmans, R.J. Heynis, P.M.A. van der Kam, and H. Verheul, Phys. Rev. C **14**, 229 (1976).

[14] D.R. LaFosse, *et al.* (unpublished).

[15] H. Harada, T. Murakami, K. Yoshida, J. Kasagi, T. Inamura, and T. Kubo, Phys. Lett. B **207**, 17 (1988).

[16] M. Ionescu-Bujor, A. Iordachescu, G. Pascovici, and C. Stan-Sion, Nucl. Phys. **A466**, 317 (1987).

[17] R. Wyss, J. Nyberg, A. Johnson, R. Bengtsson, and W. Nazarewicz, Phys. Lett. B **215**, 211 (1988).

[18] W. Satuła, R. Wyss, and F. Dönau, Nucl. Phys. **A565**, 573 (1993).

[19] C. Baktash, G. Garcia-Bermudez, D.G. Sarantites, W. Nazarewicz, V. Abenante, J.R. Beene, H.C. Griffin, M.L. Halbert, D.C. Hensley, N.R. Johnson, I.Y. Lee, F.K. McGowan, M.A. Riley, D.W. Stracener, T.M. Semkow, and A. Virtanen, Phys. Lett. B **255**, 174 (1991).

[20] I. Ragnarsson (unpublished).

[21] Y. Liang, D.B. Fossan, J.R. Hughes, D.R. LaFosse, T. Lauritsen, R. Ma, E.S. Paul, P. Vaska, M.P. Waring, N. Xu, R. Wyss, Phys. Rev. C **44**, R578 (1991); E.S. Paul, R.M. Clark, S.A. Forbes, D.B. Fossan, J.R. Hughes, D.R. LaFosse, Y. Liang, R. Ma, P.J. Nolan, P.H. Regan, P. Vaska, R. Wadsworth, M.P. Waring, J. Phys. (London) G **18**, 837 (1992); E.S. Paul, M.P. Waring, R.M. Clark, S.A. Forbes, D.B. Fossan, J.R. Hughes, D.R. LaFosse, Y. Liang, R. Ma, P. Vaska, R. Wadsworth, Phys. Rev. C **45**, R2531 (1992); E.S. Paul, J. Simpson, H. Timmers, I. Ali, M.A. Bentley, A.M. Bruce, D.M. Cullen, P. Fallon, and F. Hanna, J. Phys. (London) G **18**, 971 (1992).

[22] S. Juutinen, S. Tormanen, B. Cederwall, A. Johnson, R. Julin, S. Mitarai, J. Mukai, P. Ahonen, B. Fant, F. Liden, J. Nyberg, and I. Ragnarsson, Z. Phys. A **338**, 365 (1991); H. Timmers, J. Simpson, M.A. Riley, T. Bengtsson, M.A. Bentley, F. Hanna, S.M. Mullins, J.F. Sharpey-Schafer, and R. Wyss, J. Phys. (London) G **20**, 287 (1994).

[23] Y. Liang, R. Ma, E.S. Paul, N. Xu, and D.B. Fossan, Phys. Rev. C **42**, 890 (1990).

[24] M. Gai, D.M. Gordon, R.E. Shroy, and D.B. Fossan, Phys. Rev. C **26**, 1101 (1982).

[25] F. Dönau and S. Frauendorf, in *Proceedings of the Conference on High Angular Momentum Properties of Nuclei,*

*Oak Ridge, 1982*, edited by N.R. Johnson (Harwood Academic, New York, 1983), p. 143; F. Dönau, Nucl. Phys. **A471**, 469 (1987).

[26] V.P. Janzen, H.R. Andrews, T.E. Drake, D.B. Fossan, A. Galindo-Uribarri, B. Haas, A. Omar, D.R. LaFosse, J.R. Hughes, S. Mullins, E.S. Paul, L. Persson, S. Pilotte, D. Prévost, D.C. Radford, J. Rodriguez, M. Sawicki, H. Schnare, H. Timmers, P. Unrau, P. Vaska, J.C. Waddington, R. Wadsworth, D. Ward, J. Wilson, R. Wyss, and G. Zwartz, *Proceedings of the International Conference on Nuclear Structure at High Angular Momentum*, Canada, 1992 [AECL Report No. 10613, 1992 (unpublished)] Vol. 2, p. 333.